

# Combined prediction model for mining subsidence in coal mining areas covered with thick alluvial soil layer

Dawei Zhou<sup>1,2</sup> · Kan Wu<sup>1</sup> · Xiexing Miao<sup>2</sup> · Liang Li<sup>1</sup>

Received: 7 June 2016 / Accepted: 13 October 2016 / Published online: 7 November 2016  
© Springer-Verlag Berlin Heidelberg 2016

**Abstract** The entire overburden stratum above a coal mining area is considered to be composed of an alluvial soil layer and a bedrock layer. In underground mining, alluvial soil has a major effect on ground subsidence. This effect is especially significant and not negligible when the alluvial soil accounts for a large proportion in the entire overlying stratum of coal mining areas covered with thick alluvial soil (CMATASs). In this study, the applicability of the most popular probability integral method (PIM) used for CMATASs was analyzed, and it was found that the PIM is not suitable for ground subsidence prediction in CMATASs for two main reasons: (1) the subsidence basin range predicted by the PIM was smaller than the measured range; thus, the predicted basin converged more rapidly than the measured basin at the edges. (2) Poor fitting results were obtained at the subsidence basin edge. The mechanism of mining subsidence in CMATASs and the reasons why the PIM is not suitable for CMATASs were investigated in terms of the internal deformation and crack (void) distribution within the rock mass induced by underground coal mining. The results indicate that the alluvial soil is compacted and then subsides under vertical compression deformation, which increases ground subsidence. The bedrock is subjected to the weight/load of the thick alluvial soil layer. Because of the vertical compression deformation

inside the rock, its internal voids (spaces) are compacted; thus, the replaced voids (spaces) are transferred to the ground surface, resulting in an increase in ground subsidence. However, the effect of the alluvial soil on ground subsidence cannot be detected by the PIM; moreover, the PIM is unable to represent the mechanism of the mining subsidence in CMATASs. Thus, the PIM cannot be used for predicting subsidence in CMATASs. To precisely calculate subsidence in CMATASs, we propose a combined prediction model (CPM) for mining subsidence in CMATASs based on soil mechanics and stochastic medium theory. The new CPM was applied to the mining process in the Huainan Coal Mining Area. The calculation results show that subsidence predicted by the CPM better fits the measured subsidence values, with a relative error of 4.9%, and that the fitting accuracy is improved by 18% compared to the relative error of the PIM (6.0%). Thus, the proposed CPM is more suitable for predicting ground subsidence caused by underground coal mining in CMATASs, and can be used to provide more accurate predictions for ground subsidence in similar coal mining areas.

**Keywords** Underground mining · Mining subsidence · Alluvial soil layer · Prediction model/method · Soil mechanics

✉ Kan Wu  
dwzhou2008@gmail.com; wukan6899@263.net

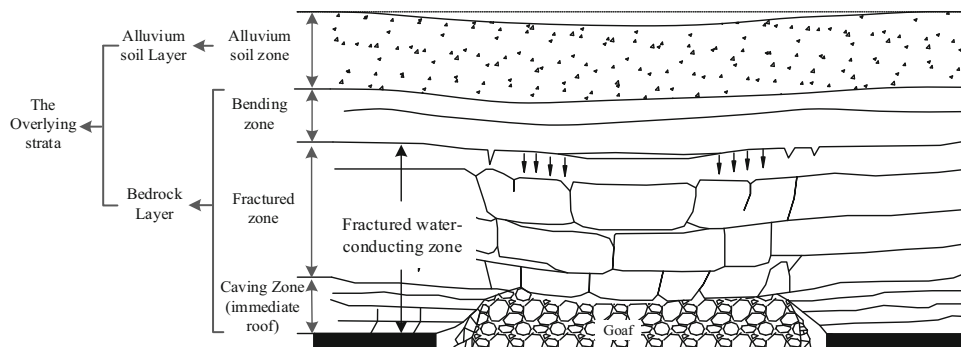
<sup>1</sup> School of Environment Science and Spatial Informatics, China University of Mining and Technology, Xuzhou, Jiangsu 221116, People's Republic of China

<sup>2</sup> State Key Laboratory for Geomechanics and Deep Underground Engineering, China University of Mining and Technology, Xuzhou 221116, China

## Introduction

In mining, after sufficient useful minerals have been extracted from a longwall panel, the original stress balance of the rock mass overlying the stope is disturbed and the overburden stratum displays various degrees of movement, causing subsidence and caving of the overlying rock mass. According to the movement characteristics, the fractured

**Fig. 1** Cross-section of four zones of strata movement above longwall goaf (Zhou et al. 2016b)



overburden stratum can be divided into four zones from the bottom to the top (Fig. 1): the caving zone, fractured zone, bending zone, and alluvial soil zone (Brady and Brown 2004; He et al. 1991; State Bureau of Coal Industry 2004; Kratzsch 1983; Miao et al. 2011; Peng and Zhang 2007; Peng 1992; Qian et al. 2003, 2010; Qian 1982; Yuan and Wu 2003). As shown in Fig. 1, the caving zone and fractured zone are jointly termed the fractured water-conducting zone (FWCZ), and the bending zone and FWCZ are jointly called the bedrock layer. Thus, the entire range of the overlying strata includes the bedrock layer and alluvial soil layer.

Alluvial soil plays an important role in ground subsidence caused by coal mining and groundwater extraction. Field-measured data show that when a coal mining area is covered with thick alluvial soil, mining subsidence in these areas shows some unique phenomena (Zhou 2014; Zhou et al. 2015, 2016a). For example, the subsidence factor is greater than 1.0 (the maximum subsidence is greater than the extracted coal seam thickness), the scope of ground subsidence is considerably wider, horizontal displacement is greater than vertical subsidence at the trough border, the active period of ground movement is more intense and concentrated, and the duration of ground movement is longer (Bureau et al. 1983; Ge and Yu 2006; He et al. 1991; State Bureau of Coal Industry 2004; Sui 1992; Tan et al. 2002; Wu et al. 1998, 1999, 2002; Yuan and Wu 2003). Consequently, studies on prediction methods for mining subsidence in coal mining areas covered with thick alluvial soil (CMATASs) have gained considerable attention.

Because of these specific characteristics of ground subsidence in CMATASs, subsidence prediction in these areas using existing prediction methods is a very difficult task. Existing prediction methods for strata and ground movements can be classified into six categories (Alejano et al. 1999; Asadi et al. 2004, 2005; Brady and Brown 2004; Cui et al. 2000b, 2001; Djameluddin et al. 2011; Holla 1997; Kratzsch 1983; Li et al. 2014; Sheorey et al. 2000; Singh and Yadav 1995; Wu et al. 1998):

- empirical methods
- influence function methods
- profile function methods
- numerical modeling methods
- theoretical modeling methods
- physical simulation methods

Although these methods have been researched by many experts in the field of mining, not all of them can be used in actual engineering projects. In China, an influence function method called the probability integral method (PIM) (Baochen and Ronggui 1981; Brady and Brown 2004; Cui et al. 2000b, 2001; He et al. 1991; Huayang et al. 2010; State Bureau of Coal Industry 2004; Kratzsch 1983; Peng 1992) is the prediction method most widely used for ground subsidence caused by underground mining. However, field-measured data show that the PIM also encounters some problems in predicting the ground subsidence in CMATASs because of its basic premise and hypothesis.

The basic hypothesis underlying the PIM is based on the sandbox model, which views the large-area of broken rock mass encountered during underground coal mining as sand. Therefore, rock mass subsidence can be studied in terms of an hourglass model. According to existing research results (Baochen and Ronggui 1981; Brady and Brown 2004; Hao 1988; Hao and Ma 1985, 1986; He 1982; He et al. 1991; State Bureau of Coal Industry 2004; Kratzsch 1983; Liu 1981; Sui 1992; Wu et al. 2013; Yuan and Wu 2003; Zhang et al. 1999), the PIM is suitable for coal mining areas covered with thin (non-)alluvial soil (N-CMATASs), and the overall calculated accuracy of the method for such areas is quite high. However, alluvial soil is different from sand and rock mass; the compressible nature of alluvial soil is in opposition to the basic premise and hypothesis of the PIM. CMATASs are distributed widely in China, concentrated mainly in the Huaibei Coal Mining Area, Huainan Coal Mining Area (HCMA), Yanzhou Coal Mining Area, Datun Coal Mining Area, Jiaozuo Coal Mining Area, Pingdingshan Coal Mining Area, Yongxia Coal Mining Area, Kailuan Coal Mining Area, Xingtai Coal Mining Area, and other mining areas in East China, Central China,

North China, and Northeast China (He et al. 1991; State Bureau of Coal Industry 2004; Liu et al. 2012; Sui 1992; Yuan and Wu 2003; Zhou 2014; Zhou et al. 2015). Therefore, it is necessary to study the mechanism of mining subsidence in CMATASs and build a more suitable prediction method for calculating subsidence in CMATASs.

Therefore, in this study, we analyzed the applicability of the PIM to CMATASs, and determined the reasons why the PIM cannot be applied to the prediction of the ground subsidence in CMATASs. Furthermore, based on the results obtained, and the mechanism of mining subsidence in CMATASs, we improved the PIM to establish a combined prediction method for predicting mining subsidence in CMATASs; this method can precisely calculate ground subsidence, evaluate the damage to ground structures caused by underground mining in CMATASs, and provide suitable control measures to prevent such damage.

### Analysis of applicability of PIM to CMATASs

The prediction model of the PIM is used to calculate the movement of an arbitrary point on the surface and express the surface subsidence trough caused by unit mining. The model can be derived as follows (Brady and Brown 2004; He et al. 1991; Kratzsch 1983; Peng 1992; Zhou et al. 2016a):

$$W_e(x) = \frac{1}{r} e^{-\frac{\pi x^2}{r^2}} \tag{1}$$

For the three-dimensional situation shown in Fig. 2, the subsidence of an arbitrary point A (x, y) on the surface caused by coal mining in unit B(s, t) is as follows:

$$W_e(x, y) = \frac{1}{r^2} e^{-\pi \frac{(x-s)^2 + (y-t)^2}{r^2}} \tag{2}$$

When the mining area is O<sub>1</sub>CDE (Fig. 2), the prediction equation for the subsidence of the arbitrary point (x, y) caused by the entire mining process is as follows:

$$W(x, y) = W_0 \int_0^l \int_0^L \frac{1}{r^2} e^{-\pi \frac{(x-s)^2 + (y-t)^2}{r^2}} dt ds, \tag{3}$$

where  $W_0 (=mqcosa)$  is the maximum subsidence value for the entire mining process;  $m$ ,  $q$ , and  $a$  represent the mining thickness, subsidence factor, and coal seam dip angle, respectively;  $r (=H_0/\tan\beta)$  is the main influence radius;  $H_0$  and  $\tan\beta$  are the average mining depth and the tangent of the main effect angle;  $l (=D_3 - S_3 - S_4)$  and  $L (=D_1 - S_1 - S_2) \times \sin(\theta_0 + a)/\sin(\theta_0)$  are the strike calculation length and dip calculation length, respectively;  $\theta_0$  is the effect transference angle; and  $S_1, S_2, S_3$ , and  $S_4$  are the left, right, raise, and dip deviations of the inflection point, respectively. The subsidence parameters are shown in Fig. 2. Details of the inversion calculation method based on the PIM can be obtained from a previous paper (Zhou et al. 2016a).

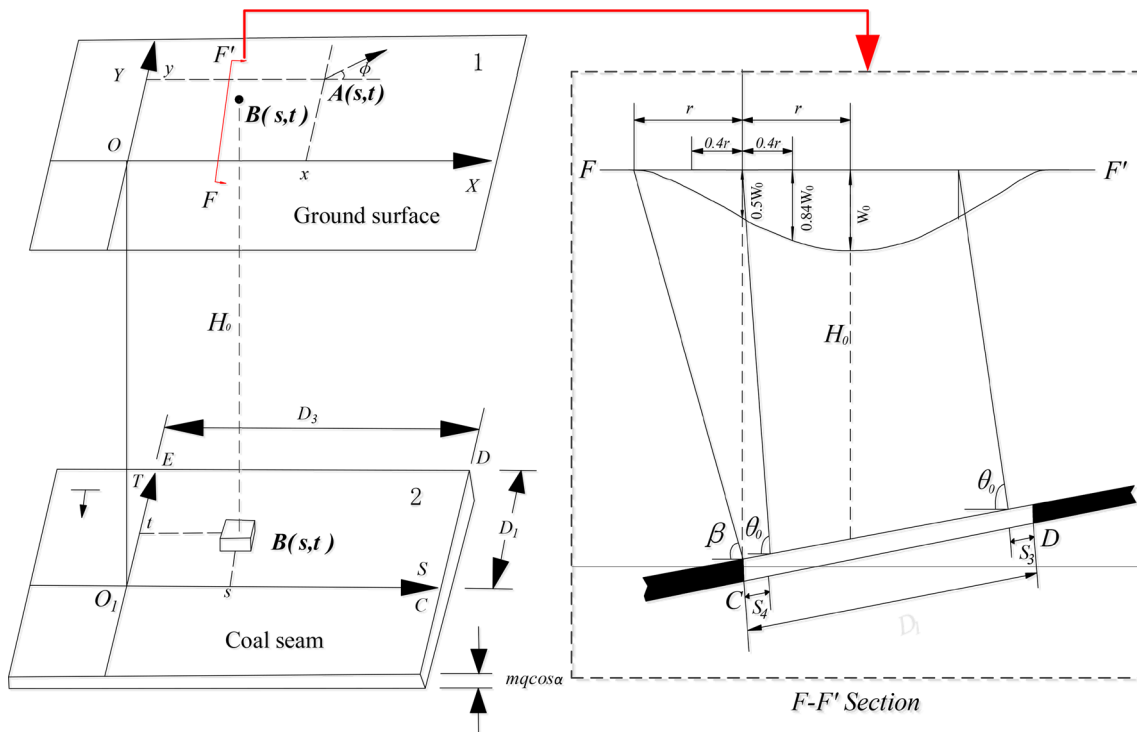
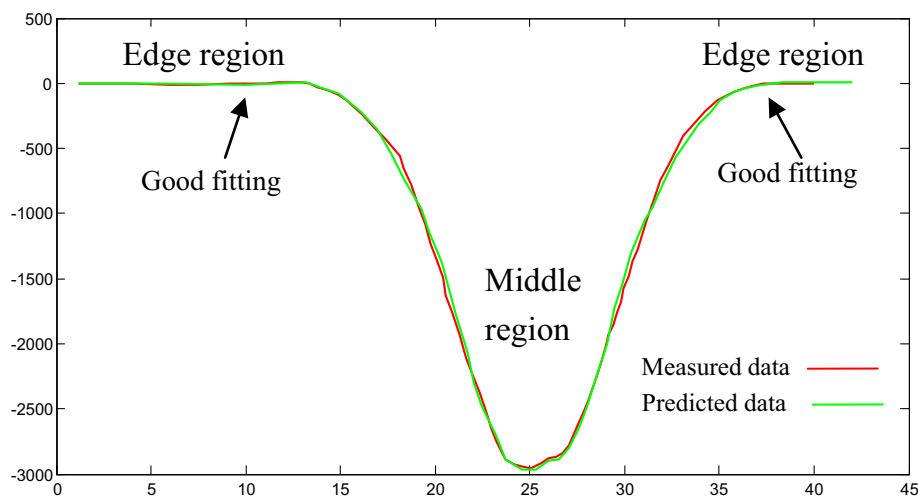
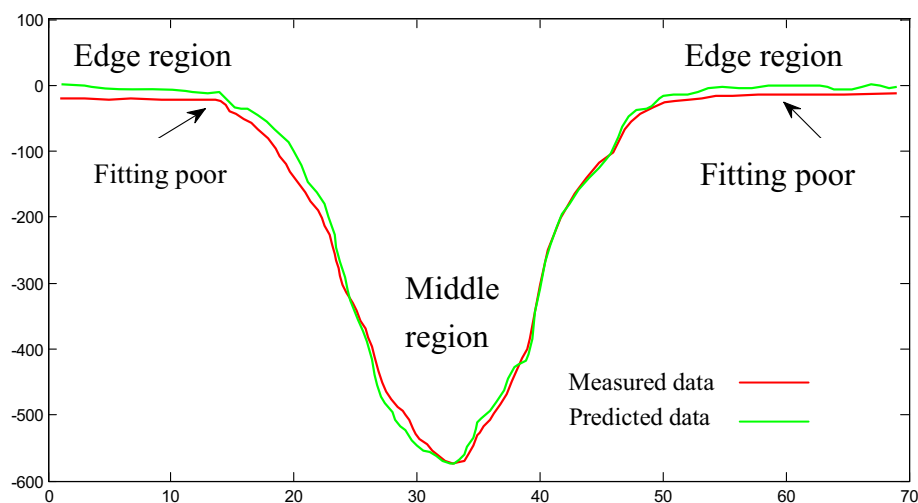


Fig. 2 Space coordinate system (1 ground surface, 2 coal seam) (Zhou et al. 2016a)

**Fig. 3** Fitting effect of measured and calculated subsidence values in South Area



**Fig. 4** Fitting effect of measured and calculated subsidence values in North Area



The PIM can be well applied to N-CMATASs; however, it cannot precisely predict the ground mining subsidence in CMATASs. We will take the HCMA as an example to analyze the problems that occur when the PIM is applied to CMATASs. The HCMA is divided into the south and north mining areas (hereinafter referred to as the “South Area” and “North Area,” respectively) by the Huai River, a major river in China located mid-way between the Yellow River and the Yangtze River. The North Area is a CMATAS, whereas the South Area is an N-CMATAS. Therefore, the HCMA shows mining subsidence characteristics of both the N-CMATAS and CMATAS (Zhou et al. 2015, 2016a).

Figure 3 shows the comparison results between the measured ground subsidence in the South Area and the fitting values obtained by the PIM. Figure 4 compares the measured subsidence in the North Area and the fitting values obtained by the PIM.

It can be seen from Figs. 3 and 4 that the prediction results by the PIM fit well to the entire sunken basin in South

Huainan, but fit poorly to the edge region in North Huainan. Moreover, the predicted basin size is smaller than the measured size, and the PIM converges rapidly at the edges.

To more exactly interpret the applicability of the PIM to predict the mining subsidence in CMATASs, subsidence data collected from 11 ground movement observation stations above the working faces in the North Area were analyzed, and the prediction results obtained by the PIM were compared with the field-measured values. The relative root mean square error was taken as the evaluation index to analyze the fitting results from each observation station (Table 1).

Root mean square error (RMSE):

$$\text{RMSE} = \sqrt{\frac{\sum_{i=1}^n \Delta_I^2}{n}} = \sqrt{\frac{\sum_{i=1}^n [W_I - (W_{\text{fm}})_I]^2}{n}}. \quad (4)$$

The relative RMSE, denoted by  $K$ , refers to the ratio of the RMSE to the maximum measured subsidence value and is given by

**Table 1** Fitting effect between field measured data and predicted data for different areas of subsidence trough

Number of working faces	Different areas of subsidence trough (ground points number)	Relative RMSE/K (%)
1	Entire region (58)	2.80
	Middle region (23)	3.82
	Edge region (35)	11.84
2	Entire region (23)	1.90
	Middle region (14)	2.31
	Edge region (9)	37.36
3	Entire region (118)	2.30
	Middle region (41)	2.47
	Edge region (77)	13.37
4	Entire region (72)	2.40
	Middle region (39)	2.99
	Edge region (33)	39.67
5	Entire region (103)	3.88
	Middle region (62)	4.51
	Edge region (41)	59.60
6	Entire region (20)	1.54
	Middle region (11)	1.36
	Edge region (9)	49.39
7	Entire region (17)	4.17
	Middle region (14)	4.56
	Edge region (3)	60.77
8	Entire region (20)	6.16
	Middle region (16)	6.87
	Edge region (4)	46.76
9	Entire region (36)	4.80
	Middle region (23)	5.86
	Edge region (13)	35.55
10	Entire region (55)	4.92
	Middle region (32)	5.25
	Edge region (23)	66.53
11	Entire region (48)	2.49
	Middle region (16)	2.84
	Edge region (32)	27.58

RMSE/K relative root mean square error

$$K = \frac{RMSE}{\text{Max}[(W_{fm})_I]}, \quad I = 1, 2, \dots, n, \quad (5)$$

where  $W_I$  is the predicted subsidence at point  $I$ ,  $(W_{fm})_I$  is the measured subsidence value at this point,  $n$  is the number of points, and  $\text{Max}[(W_{fm})_I]$  is the maximum value among the measured subsidence values.

Table 1 indicates that the PIM fitting effect is poor at the basin edges, with the maximum relative RMSE reaching up to 66.53% but is relatively good in the middle region of the subsidence basin, which indicates that the PIM is deficient in predicting the ground mining subsidence in CMATASs and

thus cannot achieve the best fitting effect. The PIM suffers from the following two main problems: (1) the predicted basin range is smaller than the measured one; thus, the PIM converges rapidly at the subsidence basin edges. (2) The fitting results at the subsidence basin edges are poor.

Compared to the conventional geological condition [thin (non-)alluvial soil layer], the alluvial soil mass accounts for a larger proportion in the entire overlying stratum in CMATASs, which affects the ground subsidence more drastically, and hence, the effect cannot be neglected. Therefore, it is difficult to precisely predict ground mining subsidence in CMATASs. In addition, CMATASs are widely distributed in China (Zhou et al. 2015, 2016a); therefore, it is necessary to build an accurate prediction model for CMATASs.

This study investigated the PIM with a view to solving the problems of predicting mining ground subsidence in CMATASs. A new combined prediction model (CPM) is proposed based on the mechanism of mining subsidence in CMATASs. The effect of alluvial soil on ground subsidence is completely considered in this new model, which further enhances the prediction accuracy for CMATASs.

### Mechanism of mining subsidence in CMATASs and reason for unsuitability of PIM for CMATASs

The alluvial soil layer has a major effect on the ground subsidence caused by underground coal mining when the alluvial soil layer accounts for a large proportion in the entire overlying stratum above a coal mining face. However, the PIM widely used in China cannot precisely predict the ground subsidence in CMATASs. In this section, we describe the inner mechanism of mining subsidence in CMATASs, and present the reasons why the PIM is not suitable for CMATASs.

### Deformation inside rock mass and alluvial soil due to underground mining

#### Measurement technique for vertical movements

Vertical movements in internal rock are monitored using the borehole extensometer system (Wu et al. 1998; Yuan and Wu 2003) shown in Fig. 5. The system consists of a probe, a cable, a cable reel with an indicating device, test tubes, an inductive loop, and a pedestal frame.

#### 1. Main components

- Probe: comprising a radio frequency oscillator and an electrical testing circuit.
- Cable: used for transmitting electrical signals generated by the probe sensor. The outer surface



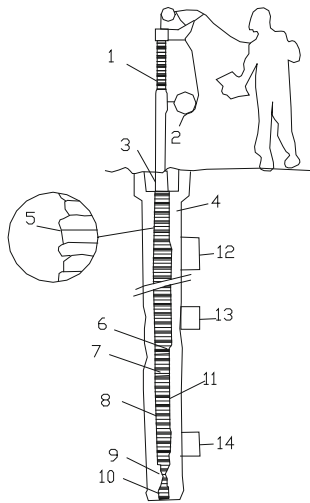


**Fig. 5** Installation diagram of subsidence measurement system (extensometer). 1—pedestal frame, 2—reading device/cable reel, 3—slurry, 4—filling mortar, 5—inductive loop sealed with adhesives and tape, 6—inductive loop, 7—inclinometer casing joints, 8—inclinometer casing, 9—grouting valve, 10—hammer, 11—probe, 12—hoseconnector fitted with adhesive and tape, 13—hose connector with nylon tape or clamp, 14—end of hose fixed with rigid tube

is marked with a scale whose least count is 1 m. The cable has an inner core, and the inner core has a cable to ensure that the cable length is not influenced by the raising or dropping of the probe.

- Cable reel with an indicating device: used for raising or dropping the probe and indicating the strength of the signal. When the probe approaches the inductive loop, the buzzer raises an alarm.
- Inclinometer tube: acts as a carrier for the inductive loop. First, an inductive loop is arranged on the test tube at regular intervals; then, the tube is placed in the borehole and filled with mortar, which causes the tube to be glued to the interior perimeter of the borehole and ensures that the inductive loop and rock move together. During observations, the probe is moved upward and downward in the test tube to determine the location of the inductive loop.
- Inductive loop: a closed loop made of metal and comprising the sensing system and probe.

- Pedestal frame: a mobile apparatus placed above the hole. The frame is scored with a millimeter scale to measure depths smaller than 1 m.

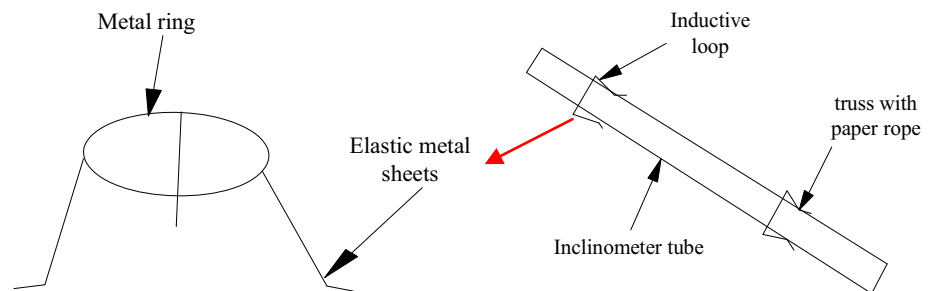
## 2. Installation

For observation holes constructed before 1992, the inductive loop was installed on a hose; the hose moved with the soil outside, as shown in Fig. 7 (2). After 1992, the inductive loop installation method was improved. The top of the inductive loop is a closed metal ring, with three resilient metal bars in the lower part. The bottom of the metal bar is folded parallel to the ring to form a small leg, as shown in Fig. 6. With this inductive loop, the plastic hose is no longer needed. During installation, the inductive loop is placed outside the PVC inclinometer tube according to the designed interval. The three legs of the induction ring are tied to the inclinometer tube using water-frangible paper rope and loaded onto the ground layer during the installation of the inclinometer tube (see Fig. 6). Upon reaching the ground layer, the paper rope breaks because of underwater soaking and the elastic force of the inductive loop legs. Thus, the inductive loop legs and the soil are joined together.

## 3. Principle of measurement

When the probe approaches the inductive loop, the sensing circuitry inside the probe triggers the buzzer to sound an alarm and causes deflection of the indicator. When the pointer reaches the peak value, i.e., when the probe is aligned exactly with the center of the inductive loop, the depth of the center of the probe can be measured using the scales on the cable and frame. Based on two measurement results obtained before and after a certain time interval, the vertical displacement of the rock strata and the vertical stretch or compression within each segment at different depths (inductive loop location) can be calculated. To obtain the absolute displacement value, at least one inductive loop (such as the one near the bottom of the hole) should be buried in a stable rock or one inductive loop (such as the one near the opening of the hole) should be measured using another method.

**Fig. 6** Improved inductive loop and its installation method



#### 4. Accuracy of the borehole extensometer system

A skilled operator can measure vertical movements up to a precision of 1.5 mm.

##### *Partition of deformation inside rock mass*

Figure 7 shows the deformation inside the bedrock and alluvial soil in different regions (Brady and Brown 2004; He et al. 1991; Kratzsch 1983; Peng 1992; Zhou et al. 2016b). As seen in Fig. 7 (2), the bedrock and soil deformation induced by underground mining can be divided into four zones:

- Zone A: a unidirectional tension–compression zone where compressive deformation occurs in the horizontal direction and tensile deformation occurs in the vertical direction.
- Zone B: a unidirectional tension–compression zone where tensile deformation occurs in the horizontal direction and compressive deformation occurs in the vertical direction.
- Zone C: a bidirectional compression zone formed by support pressure; in this zone, compression deformation occurs in both the horizontal and vertical directions.
- Zone D: a bidirectional tensile zone formed by pressure relief; in this zone, tensile deformation occurs in both the horizontal and vertical directions.

Based on the above analysis, the partition zone of vertical deformation inside the bedrock and alluvial soil can be obtained, as shown in Fig. 7 (3). The vertical deformation inside the bedrock and alluvial soil is divided into two regions fringed by the inflection point:

- Region I: vertical tensile deformation zone.
- Region II: vertical compression deformation zone.

#### **Distribution of fracture interspace in rock mass caused by underground mining**

Figure 8a shows a binary image of only mining-induced fracture interspaces in the overlying stratum. The image was obtained by processing the original digital image using binarization enhancement using the region histogram method. Figure 8b shows the distribution of the fracture interspace density along the direction of the coal seam according to the fracture measurements, and statistics in the horizontal and vertical directions shown in Fig. 8a. According to the field-measured data, we drew a contour of the fracture interspace distribution in the Taoyuan mine of the Huaibei Coal Mining Area (Fig. 9) when the mining distance of the working face is 250 m. The figure shows the plane distribution feature of the internal space of the rock

mass (Qian et al. 2003). The following conclusions can be obtained from Figs. 8 and 9:

1. The mining-induced fracture interspaces inside the overlying rock are distributed mainly in three areas:
  - (a) Region ① in Fig. 8a: inside the rock mass located on the top of the mining start line.
  - (b) Region ② in Fig. 8a: the internal rocks located on the top of the mining terminal line.
  - (c) Region ③ in Fig. 8a: the internal rocks located in the middle and lower area above the goaf.

In addition, we can see region ④ in Fig. 8a, which is in the middle part of the mining area. However, the fracture interspace located in the upper area above the goaf is closed; therefore, no fracture interspaces appear in the area. From the analysis in Sect. [Deformation Inside Rock Mass and Alluvial Soil Due to Underground Mining](#), we can infer that regions ① and ② in Fig. 8a are the same as region II in Fig. 7 (3), namely, the vertical compression deformation zone.

2. With an increase in the height to the coal seam, the fracture interspace density gradually decreases. The density of the fracture interspace on both the sides of the goaf area is greater than that in the middle part above the goaf area, as shown in Fig. 8b.
3. After underground mining, a horizontally connected mining-induced fracture interspace region exists along the different levels of rock mass around the goaf area. The distribution of the projection to the ground surface is shown in Fig. 9, which is called the “O” ring distribution of the mining-induced fracture.

#### **Comprehensive analysis and discussion**

##### *Compacting subsidence of alluvial soil mass*

Alluvial soil is composed of loose particles and is a three-phase medium consisting of soil particles, gas, and water (Gong 1996), as shown in Fig. 10. According to the effective stress principle (Gong 1996; Sui 1992; Yin 2007), the water and gas in the alluvial soil are squeezed under the additional compressive stress generated by the disturbance due to underground mining, causing relative sliding and displacement among soil particles (i.e., changes in the arrangement of soil particles). Soil particles move close to each other, causing pore volume changes and soil compression deformation.

Under the influence of vertical compressive deformation from region II shown in Fig. 7 (3), the water and gas in the gaps of the alluvial soil mass are squeezed out; thus, soil particles contact each other more closely and the volume of

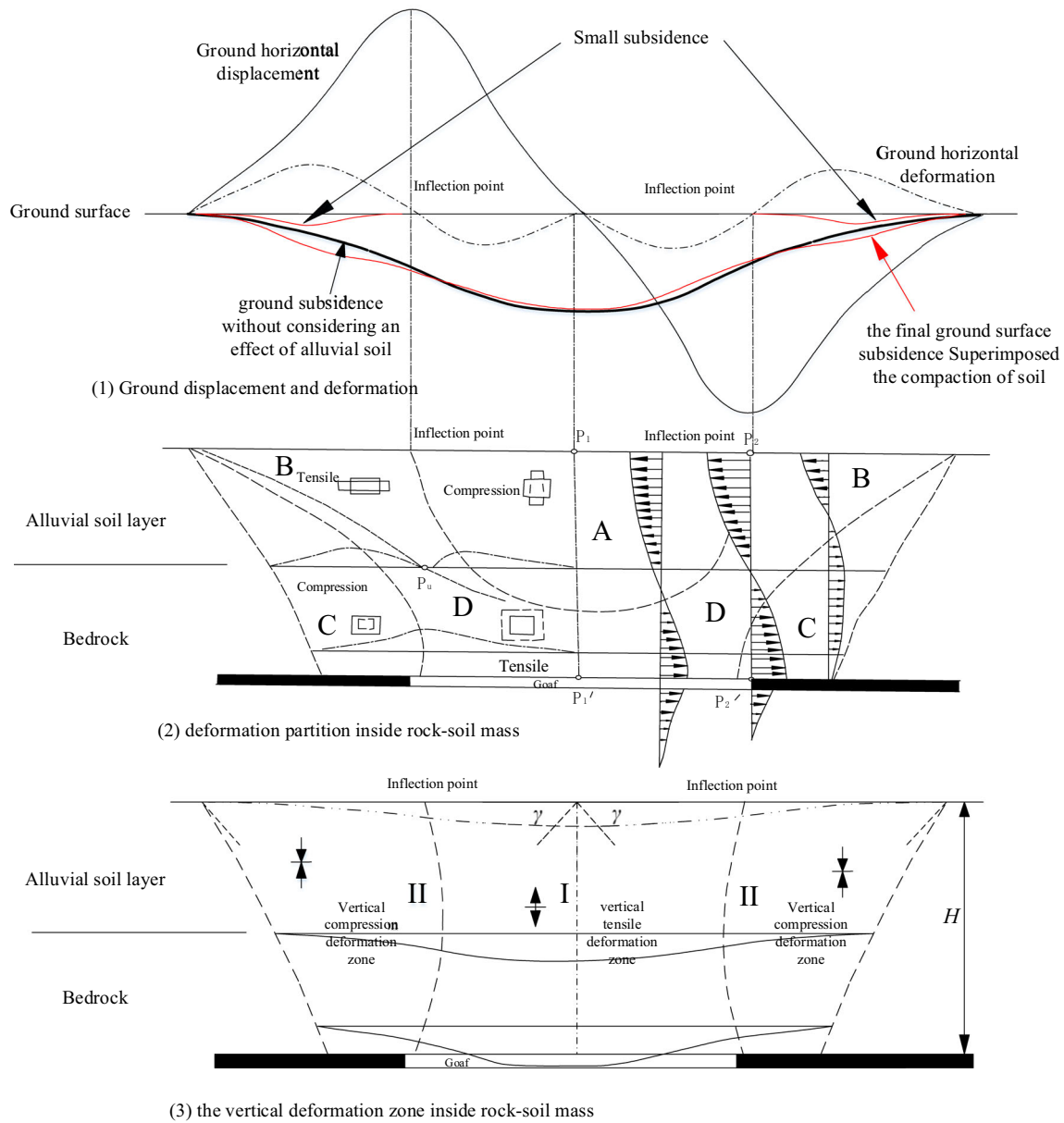


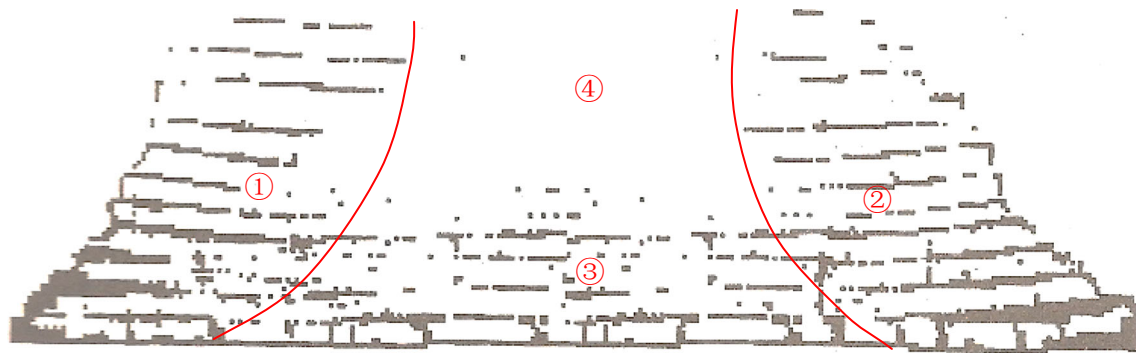
**Fig. 7** Horizontal and vertical deformation inside overlying bedrock and alluvial soil

soil is reduced, causing vertical compacting subsidence of the alluvial soil in region II. The compressed soil void is transferred to the surface, which causes additional subsidence, thus increasing the ground surface subsidence, thus increasing the ground surface subsidence. Zone B in Fig. 7 (2) indicates that the horizontal tensile deformation corresponds to the vertical compression deformation. Therefore, the additional ground subsidence from the compaction of the alluvial soil emerges at the subsidence basin edge. The additional small basins from the compacting subsidence are shown by the red curve in Fig. 7 (1). The figure indicates that the maximum compacting subsidence value is reached at the maximum horizontal deformation.

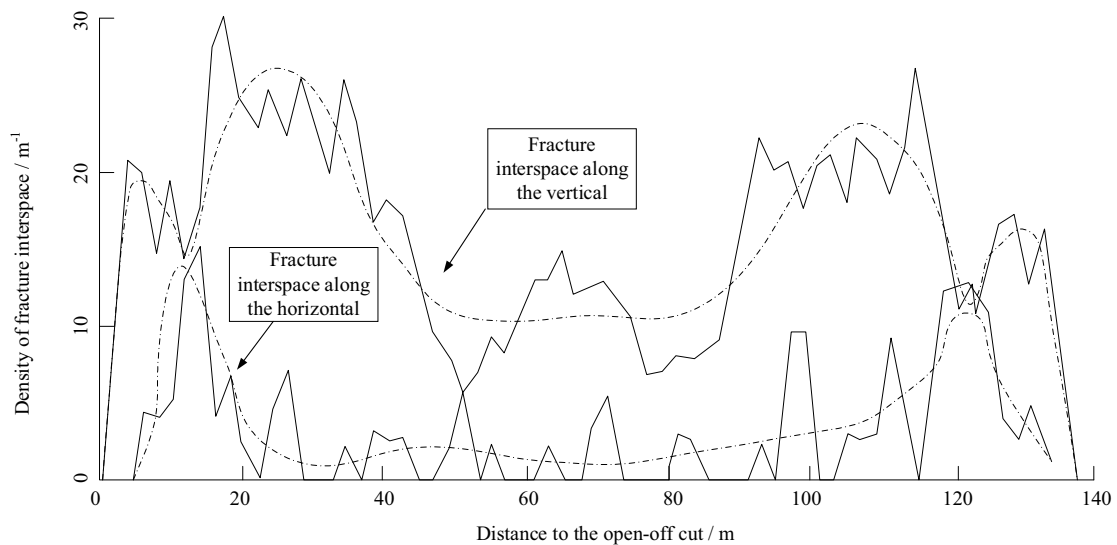
#### *Synergy subsidence from compacted fracture interspace*

According to the analysis results presented in [Distribution of Fracture Interspace in Rock Mass Caused by Underground Mining](#), regions ① and ② in Fig. 8a are almost the same as region II in Fig. 7 (3). Moreover, the overlying bedrock is covered by thick alluvial soil, and the thick alluvial soil impacts the fracture interspace inside the rock mass in the form of a load. Because of the alluvial soil load and vertical compressive deformation in zone II shown in Fig. 7 (3), the bedrock separates and the fracture interspaces in regions ① and ② shown in Fig. 8a are further compacted. The compacted rock space is replaced and





(a) Mining-induced fracture interspace in rock mass image obtained after binary processing



(b) Density distribution of mining-induced fracture interspaces

**Fig. 8** Mining-induced fracture interspace distribution characteristics inside bedrock along strike direction of working face (Qian et al. 2003)

transferred to the ground surface in the form of subsidence, thus increasing the ground surface subsidence. The synergy subsidence mainly occurs in the overlying rock gap surrounding the goaf.

The final ground surface subsidence basin can be obtained based on the superposition principle and is shown by the red curve in Fig. 7 (1). However, the PIM cannot detect the additional small basins formed at the subsidence basin edge. This is the intrinsic reason why the PIM converges more rapidly at the edge of the subsidence basin and has poor calculation accuracy in predicting the subsidence in CMATASs.

*Mechanism of mining subsidence in CMATASs*

According to the above analysis and previous research results (Zhou 2014; Zhou et al. 2015, 2016a, b), mining-induced ground subsidence is the joint result of the

movements of the overlying bedrock and alluvial soil masses. As two different media, the bedrock mass and alluvial soil play different roles in affecting ground subsidence (Zhou et al. 2015): (1) due to the bulking of broken rock mass and its strong bearing capacity, rock masses reduce subsidence to a certain extent. (2) Because of compaction in shallow regions and consolidation caused by water loss in deep regions, the alluvial soil mass increases ground subsidence. (3) The synergy effect of the two media increases ground subsidence to a certain extent. The combined effect of these three movements eventually causes the formation of the ground subsidence basin. According to the analysis illustrated in Fig. 11, the ground surface subsidence ( $W$ ) in CMATASs consists of four parts: (1) the subsidence of the alluvial soil following the bedrock subsidence caused by coal mining ( $W_f$ ), (2) the subsidence due to groundwater loss and consolidation of the alluvial soil in the coal mining area ( $W_l$ ), (3) the

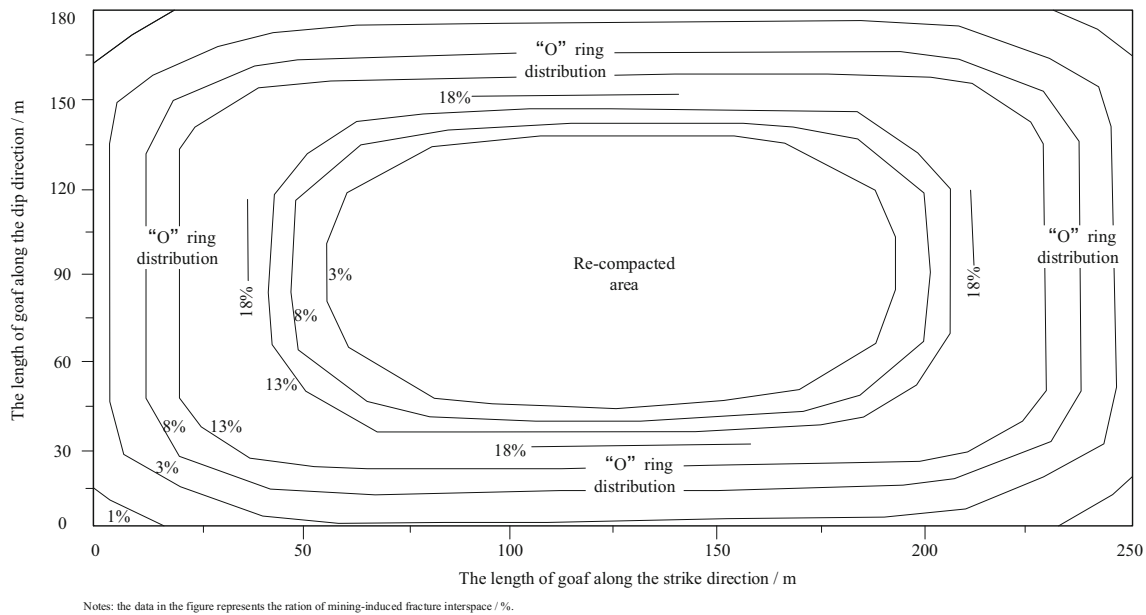


**Fig. 9** “O” ring distribution of mining-induced fracture interspace (Qian et al. 2003)

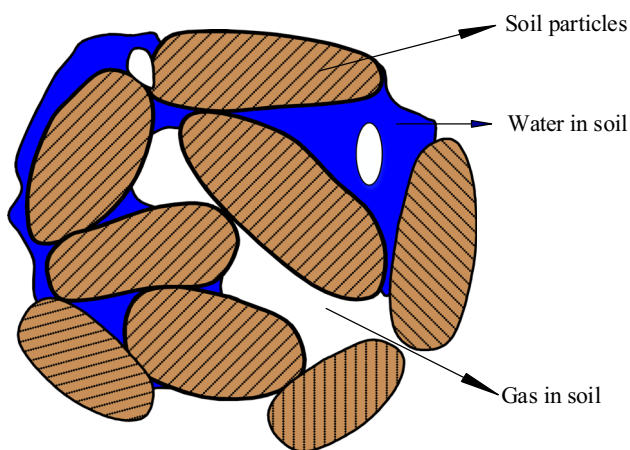


**Fig. 10** Composition of soil (Gong 1996)

compacting subsidence of shallow soil under the disturbance of coal mining ( $W_c$ ), and (4) the synergy subsidence between the alluvial soil and bedrock ( $W_s$ ). Therefore, the following formula is obtained:

$$W = W_f + W_1 + W_c + W_s, \quad (6)$$

where  $W_1$  and  $W_c$  are together called the additional subsidence of the soil itself and are caused by the deformation of the soil layer under the influence of underground mining.

We define the ratio of the alluvial soil thickness to bedrock layer thickness as the soil-to-rock ratio, and use it as a standard to evaluate the effect of the alluvial soil on the ground subsidence. If the alluvial soil layer is sufficiently thin (i.e., generally, if the soil-to-rock ratio is approximately 0.05–0.1), the sum of  $W_1$  and  $W_c$  will be too small to change the ground subsidence, and the influence of the alluvial soil

layer on the ground subsidence can be ignored. However, when the alluvial soil layer is sufficiently thick [i.e., when the soil-to-rock ratio is greater than 0.5 (Zhou et al. 2016b)], the subsidence of the soil itself ( $W_1$  and  $W_c$ ) will be sufficiently large to change the ground subsidence. In addition, thick alluvial soil influences the goaf in the form of a load, which makes the fractured rock mass in the goaf to become more compacted and the separated layer to become more closed. The displaced rock gap (space) is transferred to the bedrock surface in the form of subsidence, which increases the bedrock surface subsidence and further increases the earth surface subsidence; such subsidence is called the synergy subsidence between the alluvial soil and bedrock ( $W_s$ ) (Zhou et al. 2016b). Therefore, the thick alluvial soil layer will obviously affect the ground subsidence, including the value and the shape of the subsidence. This is the reason why some unique subsidence phenomena are expected to occur in these CMATASs.

In this study, based on the mechanism of ground surface subsidence in CMATASs, a CPM was established, in which the influence of the alluvial soil on ground surface subsidence has been sufficiently considered, so as to improve the subsidence prediction accuracy for CMATASs and similar mining areas.

## Combined prediction model

### Fundamental hypothesis

According to the actual situation of the alluvial soil and the modeling needs, the following assumptions were made:

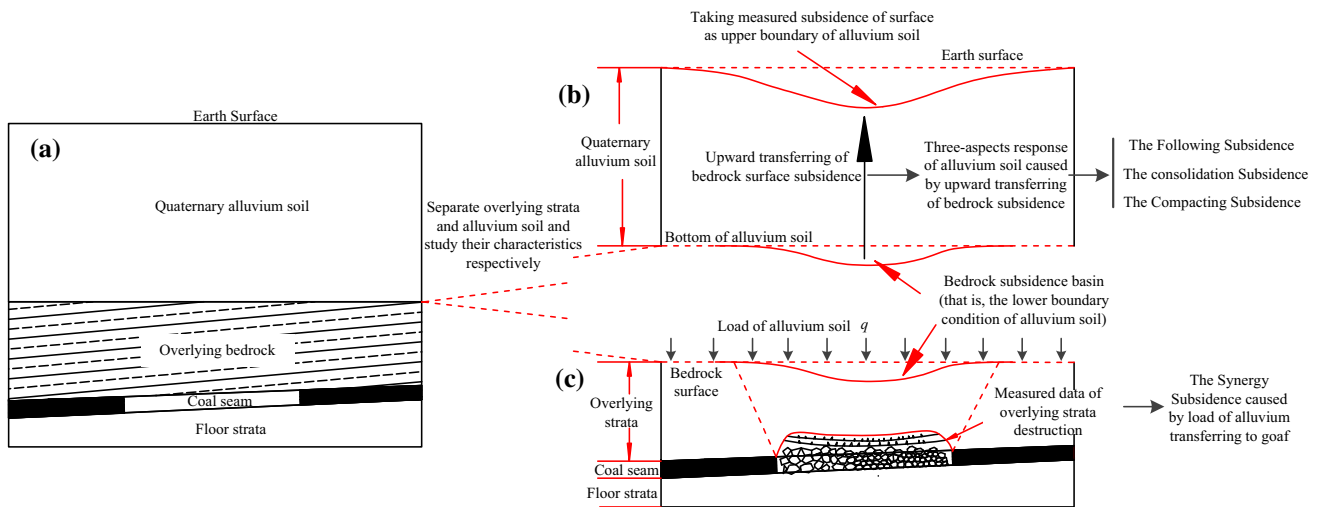


**Fig. 11** Mechanism of ground surface subsidence in coal mining areas covered with thick alluvial soil (CMATASs) (Zhou et al. 2015)

1. Assuming that the alluvial soil above groundwater level is unsaturated and contains a three-phase medium, within the scope of influence of underground mining, the ground surface subsidence caused by water and air being squeezed out by an increase in the additional stress of the soil mass because of underground mining is defined as the compacting subsidence of the soil mass.
2. Assuming that the alluvial soil below groundwater level is saturated and contains a two-phase medium (consisting of soil particles and water), within the scope of influence of mining, the consolidation subsidence of the soil mass is defined as the subsidence caused by the water loss contained in soil voids.
3. According to the above analysis, the PIM cannot detect the additional subsidence of the alluvial soil layer. When we predict the ground subsidence using the PIM, which is equal to considering the thick alluvial soil layer as a rock mass, the load of the alluvial soil is approximately substituted by a rock mass load of the same thickness. When we calculate the subsidence up to the ground surface using the PIM, in the calculation results, the predicted subsidence certainly contains the following subsidence and synergy subsidence.

**Calculation principle and method**

The CPM should include the four parts of subsidence considered in the analysis in “Comprehensive Analysis and Discussion”. The calculation principles are as follows: the alluvial soil mass is regarded as an incompressible rock mass, and the probability integral is used to predict the ground surface subsidence. The prediction results include the following subsidence ( $W_f$ ) and synergy subsidence

( $W_s$ ). If we can deduce formulas and calculate the compacting subsidence of the shallow alluvial soil mass ( $W_c$ ) and consolidation subsidence of the deep soil mass ( $W_1$ ), then, according to the superposition principle, the CPM that contains the above four parts of subsidence can be obtained.

1. Consider the alluvial layer as a rock mass; the ground surface subsidence ( $W_{fs} = W_f + W_s$ ) is directly estimated by the PIM.
2. Calculate the compacting subsidence of the shallow soil mass ( $W_c$ ) and consolidation subsidence of the deep soil mass ( $W_1$ ).

According to the superposition principle, the following CPM for mining subsidence that includes all the above four parts of subsidence is obtained:

$$W = W_{fs} + W_c + W_1. \tag{7}$$

**Establishment of CPM**

Based on Eq. (7),  $W_{fs}$  can be calculated by the PIM using Eq. (3) given in “Analysis of Applicability of PIM to CMATASs”. The calculation equations for the compacting subsidence of the shallow soil mass ( $W_c$ ) and consolidation subsidence of the deep soil mass ( $W_1$ ) are deduced as follows.

*Compacting subsidence of shallow soil under disturbance of underground coal mining ( $W_c$ )*

According to soil mechanics (Gong 1996; Yin 2007), by employing the method for calculating layering summation, the total compacting subsidence can be determined as the sum of the compacting subsidence of each soil layer:

$$W_c = \int_0^h \varepsilon_z dz, \tag{8}$$

where  $\varepsilon_z$  is the vertical deformation and is a function of  $(x, z)$ , and  $h$  is the thickness of the alluvial soil above the groundwater level.

Based on elastic mechanics (Xu 2006), the material volumetric strain  $e$  can be presented as the sum of the linear strains  $\varepsilon_x$ ,  $\varepsilon_y$ , and  $\varepsilon_z$  along the three axes:

$$e = \varepsilon_x + \varepsilon_y + \varepsilon_z. \tag{9}$$

Under a two-dimensional plane condition (Brady and Brown 2004; He et al. 1991; Kratzsch 1983), Eq. (9) can be changed into

$$\varepsilon_x + \varepsilon_z = 0. \tag{10}$$

According to the equation of elastic mechanics, we have

$$\begin{aligned} \varepsilon_x &= \frac{\partial U_e(x, z)}{\partial x}, \\ \varepsilon_z &= -\frac{\partial W_e(x, z)}{\partial z}. \end{aligned} \tag{11}$$

From Eqs. (10) and (11), we have

$$\frac{\partial U_e(x, z)}{\partial x} = \frac{\partial W_e(x, z)}{\partial z}. \tag{12}$$

Here,  $U_e(x, z)$  represents the horizontal displacement of the internal point  $(x, z)$  of the rock-soil mass due to unit mining, which is concisely called the unit horizontal displacement.  $W_e(x, z)$  is the unit subsidence trough at the  $z$  level.  $\varepsilon_x$  represents the horizontal deformation, and  $\varepsilon_z$  represents the vertical deformation; in the equation of  $\varepsilon_z$ , “-” represents the direction of the  $W$  axis, which is opposite to that of the  $z$  axis.

According to stochastic medium theory (Brady and Brown 2004; He et al. 1991; Kratzsch 1983),

$$W_e(x, z) = \frac{1}{r_z} e^{-\frac{\pi x^2}{r_z^2}}. \tag{13}$$

According to Eqs. (12) and (13), the calculation equation for the internal compression deformation  $\varepsilon_z(x, z)$  of the rock-soil mass along the  $z$  direction is

$$\varepsilon_z(x, z) = \frac{2\pi b_z W_0}{r_z^2} x e^{-\frac{\pi x^2}{r_z^2}}. \tag{14}$$

Therefore, Eq. (8) can be written as

$$W_c = \int_0^h \frac{2\pi b_z W_0}{r_z^2} x e^{-\frac{\pi x^2}{r_z^2}} dz \tag{15}$$

Here,  $r_z$  and  $b_z$  represent the major influence radius and horizontal displacement coefficient at the  $z$  level, respectively.

By discretizing Eq. (15), the following equation is obtained:

$$W_c = \sum_{i=1}^n \varepsilon_i h_i = \sum_{i=1}^n \frac{2\pi b_i (W_0)_i}{r_i^2} x e^{-\frac{\pi x^2}{r_i^2}} h_i, \tag{16}$$

where  $W_c$  is the total compacting subsidence of the shallow soil mass,  $n$  is the number of soil layers,  $h_i$  is the thickness of the  $i$ th soil layer,  $b_i$  and  $r_i$  are the probability integral parameters on the  $i$ th soil layer, and  $(W_0)_i$  is the maximum subsidence of the  $i$ th soil layer.

Therefore, for the shallow soil mass above the groundwater level, the horizontal deformation of the ground surface can be used as the vertical compression deformation value, and the soil layer number  $n = 1$ ; thus, the equation for the compacting subsidence of the shallow soil mass  $W_c$  is

$$W_c = \varepsilon(x)h = \frac{2\pi b W_0}{r^2} x e^{-\frac{\pi x^2}{r^2}} h, \tag{17}$$

where  $r$  is the main influence radius defined in “Analysis of applicability of PIM to CMATASs”, and  $b$  is the horizontal coefficient of the ground surface.

*Consolidation subsidence due to groundwater loss of deep alluvial soil in CMATASs ( $W_l$ )*

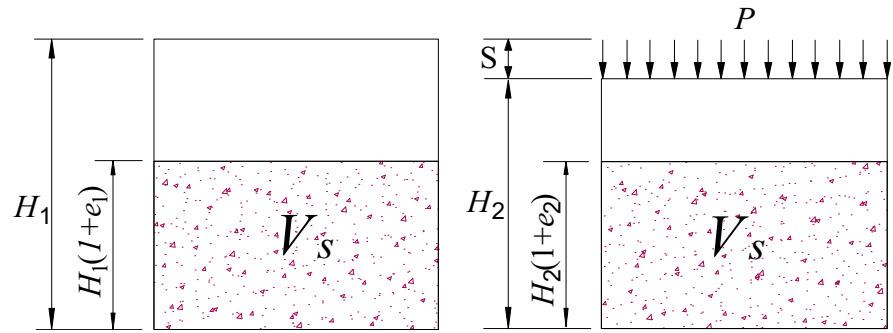
A decline in the groundwater level due to water loss causes alluvial soil consolidation and thereby results in ground surface subsidence; this phenomenon is observed in both mining and non-mining areas, and has been confirmed by a large number of measurements. Based on soil mechanics (Gong 1996; Yin 2007) and stochastic medium theory (Baochen and Rongui 1981; Brady and Brown 2004; He et al. 1991; Kratzsch 1983; Litwiniszyn 1956, 1974; Peng 1992; Reddish and Whittaker 2012), the calculation equation for the ground surface subsidence caused by water loss and consolidation of deep soil masses has been deduced.

*Compression characteristics of soil mass* Assume that, before the compressive stress  $\Delta p$  is applied, the height of a specimen is  $H_1$  and the void ratio is  $e_1$ ; after applying the compressive stress  $\Delta p$ , the compression deformation of the specimen is  $S$ , the height is  $H_2$ , and the void ratio is  $e_2$ , as shown in Fig. 12. Then, the soil particle size  $V_{s1}$  before applying the compressive stress and  $V_{s2}$  after applying the compressive stress are

$$V_{s1} = \frac{1}{1 + e_1} H_1 A_1, \tag{18}$$

$$V_{s2} = \frac{1}{1 + e_2} H_2 A_2 = \frac{1}{1 + e_2} (H_1 - S) A_2. \tag{19}$$

**Fig. 12** Sketch map of soil compression



Throughout the deformation process before and after compression, the soil particle size and basal area of the soil sample remain unchanged, namely,  $A_1 = A_2$  and  $V_{s1} = V_{s2}$ ; thus, after summarization, we have

$$S = \frac{-\Delta e}{1 + e_1} H_1, \tag{20}$$

$$\Delta e = e_2 - e_1.$$

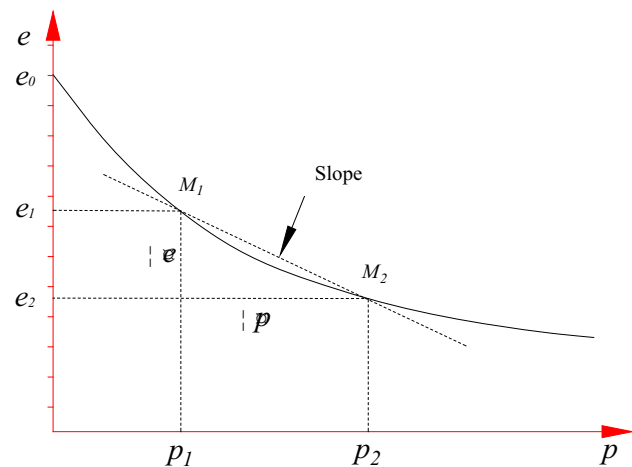
When the initial stress  $P$  is given,  $e_1$  and  $H_1$  can be determined.  $\Delta e$  indicates the change in the void ratio of the rock-soil mass; thus,  $S$  is a single-valued linear function of  $\Delta e$ . After determining the value of  $\Delta e$ , the subsidence of the soil mass can be calculated.

Figure 13 shows the  $e-p$  curve; the slope of any point on the curve indicates the compressibility of soil under pressure  $p$ .

$$a = -\frac{de}{dp}, \tag{21}$$

here, “-” indicates that  $e$  gradually decreases with an increase in pressure  $p$ . In the compression curve, the secant slope is used to represent the soil compressibility, which is

$$a = -\frac{de}{dp} \approx -\frac{\Delta e}{\Delta p} = \frac{e_1 - e_2}{p_2 - p_1}, \tag{22}$$



**Fig. 13** Sketch map of soil compression coefficient

where  $a$  is the compression coefficient ( $\text{KPa}^{-1}$  or  $\text{MPa}^{-1}$ ) of the soil mass; the void ratio change caused by a unit pressure increment is used to represent soil compressibility. Hence, Eq. (22) can be written as

$$-\Delta e = a \times \Delta p = a(p_2 - p_1). \tag{23}$$

*Consolidation subsidence of deep soil mass* As shown in Fig. 14, let  $h$  be the groundwater level before water loss due to underground mining, and assume that the rock-soil masses below the groundwater level are saturated. For the plane unit  $d\zeta d\eta$  at the depth of  $\eta$ , the unit stress is

$$p = h\gamma_s + (\eta - h)\gamma_{\text{sat}}, \tag{24}$$

where  $\gamma_s$  is the bulk density of the unsaturated rock-soil mass above the groundwater level, and  $\gamma_{\text{sat}}$  is the bulk density of the saturated soil-rock mass.

The void water pressure of the saturated soil mass is

$$p_w = (\eta - h)\gamma_w, \tag{25}$$

where  $\gamma_w$  is the bulk density of the void water.

The stress of the rock-soil particles is

$$\sigma = p - p_w = h\gamma_s + (\eta - h)(\gamma_{\text{sat}} - \gamma_w). \tag{26}$$

The void water pressure after water loss will be borne by the rock-soil particles; consequently, the stress of the rock-soil particles increases, and the stress increment of the rock-soil particles is  $\Delta p = p_w = (\eta - h)\gamma_w$ .

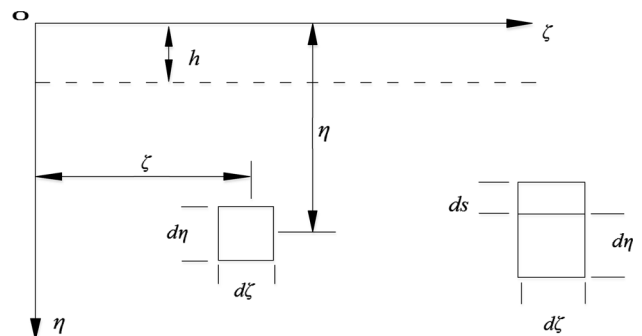


**Fig. 14** Model of consolidation due to water loss in deep saturated soil (Cui et al. 2000a; Liang et al. 2007)



According to the compression properties of the rock-soil mass, the micro-compression produced by the unit  $d\zeta d\eta$  under the action of the stress increment  $\Delta p$  can be deduced from Eq. (20) as

$$ds = \frac{-\Delta e}{1 + e_1} d\eta. \tag{27}$$

Based on Eq. (23), we can obtain the following formula:  
 $-\Delta e = a \times \Delta p = a(\eta - h)\gamma_w.$  (28)

According to random medium theory (Baochen and Ronggui 1981; Litwinski 1956, 1974), after the water loss of the soil mass, the micro-subsidence  $ds$  due to the soil mass water loss will cause the displacement of the rock-soil mass above its unit. Assume that the displacement is  $d_{\text{water}}(x)$  and the displacement of the rock-soil mass above the entire unit  $d\eta$  due to its subsidence is  $d_{\text{water}}(-x) + dw(x)$ . Here,  $dw(x)$  indicates the micro-displacement of the overlying rock-soil mass without considering the ground surface subsidence caused by the water loss. Therefore, the following equation is established:

$$d_{\text{water}}(x) = \frac{-\Delta e}{1 + e_1} (d_{\text{water}}(x) + dw(x)). \tag{29}$$

The above equation can be summarized as

$$d_{\text{water}}(x) = \frac{-\Delta e}{1 + e_1 + \Delta e} dw(x). \tag{30}$$

By integrating both the sides of Eq. (30), we have

$$w_{\text{water}}(x) = \frac{-\Delta e}{1 + e_1 + \Delta e} w(x). \tag{31}$$

According to the PIM, the calculation equation for the subsidence of any point A on the ground surface caused by semi-infinite unit thickness mining is

$$w_e(x) = \int_0^\infty \frac{1}{r} e^{-\pi \frac{(x-s)^2}{r^2}} ds. \tag{32}$$

If the mining thickness is  $m$ , the calculation equation for the subsidence of any point A on the ground surface caused by semi-infinite mining is

$$w(x) = W_0 \int_0^\infty \frac{1}{r} e^{-\pi \frac{(x-s)^2}{r^2}} ds. \tag{33}$$

By substituting Eq. (33) into Eq. (31), we have

$$w_{\text{water}}(x) = \frac{-W_0 \times \Delta e}{1 + e_1 + \Delta e} \int_0^\infty \frac{1}{r} e^{-\pi \frac{(x-s)^2}{r^2}} ds. \tag{34}$$

By applying the probability integral function erf, Eq. (34) can be written as

$$w_{\text{water}}(x) = \frac{-W_0 \times \Delta e}{2(1 + e_1 + \Delta e)} \left[ \text{erf}\left(\frac{\sqrt{\pi}}{r} x\right) + 1 \right], \tag{35}$$

where  $W_0$  is the maximum subsidence of the ground surface,  $a$  is the inclination of the coal seam,  $m$  is the mining

thickness, and erf is the probability integral function,  $\text{erf}\left(\frac{\sqrt{\pi}}{r} x\right) = \frac{2}{\sqrt{\pi}} \int_0^{\frac{\sqrt{\pi}}{r} x} e^{-u^2} du$ , which can be solved by looking up the probability integral table (He et al. 1991; State Bureau of Coal Industry 2004; Peng 1992).

Therefore, the calculation equation for the ground surface subsidence  $W_1$  as a reflection of the soil mass consolidation caused by deep soil mass dehydration is

$$W_1 = \frac{-W_0 \times \Delta e}{2(1 + e_1 + \Delta e)} \left[ \text{erf}\left(\frac{\sqrt{\pi}}{r} x\right) + 1 \right]. \tag{36}$$

*Prediction formula of CPM*

Through the above analysis, according to the principle of superposition, the prediction formula of the CPM for the subsidence in CMATASs along the major section of the subsidence trough in the strike direction is

$$\begin{aligned} W(x) &= W_{\text{fs}} + W_c + W_l \\ &= \frac{W_0}{2} \left[ \text{erf}\left(\frac{\sqrt{\pi}}{r} x\right) + 1 \right] + \frac{2\pi b h W_0}{r^2} x e^{-\pi \frac{x^2}{r^2}} \\ &\quad + \frac{-W_0 \Delta e}{2(1 + e_1 + \Delta e)} \left[ \text{erf}\left(\frac{\sqrt{\pi}}{r} x\right) + 1 \right]. \end{aligned}$$

By summarizing the above equation, we obtain

$$\begin{aligned} W(x) &= \frac{2\pi b h W_0}{r^2} x e^{-\pi \frac{x^2}{r^2}} \\ &\quad + \frac{W_0(1 + e_1)}{2(1 + e_1 + \Delta e)} \left[ \text{erf}\left(\frac{\sqrt{\pi}}{r} x\right) + 1 \right], \end{aligned} \tag{37}$$

where  $b$  is the horizontal displacement coefficient,  $h$  is the shallow soil mass thickness (namely, the depth of the groundwater level),  $e_1$  is the void ratio of the soil mass before mining disturbance, and  $\Delta e$  is the change in the ratio of the rock-soil mass before and after the mining disturbance.

Equation (37) is the prediction equation of the CPM, which completely considers the influence of the alluvial soil mass on mining subsidence. In addition to the three parameters related to alluvial soil, the CPM still uses the eight parameters of the PIM. Although the parameters of the CPM and PIM are the same, when applied to CMATASs, the actual components of the parameters are different.

**Application of CPM to CMATAS from HCMA and associated analysis**

**General situation**

The length along the strike direction of the 1212(3) working face of the Pansan Mine in the HCMA is approximately 640 m, the length along the dip direction is approximately 140 m, and the elevation of the mine roadway ranges from

–497.3 to –505.1 m. The elevation of the bedrock surface (a rough interface between the alluvial soil layer and bedrock) ranges from –396 to –411 m, the thickness of the alluvial soil layer ranges from 420 m to 440 m, and the bedrock thickness is approximately 100 m. Mining on this face, which was launched on 21 April 1999, and closed on 18 October 1999, lasted for nearly 6 months. The average mining speed was approximately 106 m per month, and the average mining height was 2.9 m. Figure 15 is the borehole log of the Pansan Mine in the HCMA, and shows the geologic conditions of their examined area.

### Mining subsidence monitoring using leveling measurement

We built a ground observation station above the working face and monitored the ground subsidence by leveling measurement. The design principles of the ground observation station and measurement method (Zhou et al. 2015, 2016a) were as follows:

#### 1. Design principles of observation station

To obtain more accurate, reliable, and representative observation data, the design of observation stations should follow these principles:

- The observation line should be located in the main section of the basin ground movement.
- The observation line length should be greater than the range of the ground basin movement.
- The measurement points of the observation line should have a certain density, depending on the depth of the mine and the purpose of the observation station.
- The control point of the observation stations should be set outside the range of the moving basin and should be firmly embedded. In permafrost regions, the bottom of the control point should be below 0.5 m from the frozen soil line.

Based on the abovementioned criteria, a ground movement observation station that included two observation lines along the strike and dip directions was built on the ground surface above the 1212(3) working face. The observation line length along the strike direction was 1268 m, containing 38 observation points, and the observation line length along the dip direction was 1150 m, containing 31 observation points, as shown in Fig. 16. By comparing the observed affected area with the calculated affected area, it can be verified that the reference points are outside the mining sphere and are not affected by mining.

#### 2. Leveling requirements and implementation

If both the ends of the observation line are set using those control points, a leveling measurement is initiated from a control point of one end of the observation station,

then matched to a control point at the other end of the observation station. If there is only one control point at one end of the observation line, a round trip measurement is required. Because the platform of the 1212(3) working face has only one control point, a round trip observation is adopted. The precision of the observation was in accordance with the third level of national accuracy requirements, and the elevation at each measurement point was adjusted and calculated. Based on the first and last observations, a final subsidence value was obtained. The field monitoring data are listed in Table 2.

### Application analysis of CPM

According to the measured data, the PIM (Zhou et al. 2016a) and CPM were used separately for the inverse analysis to calculate the measured parameters, which are listed in Table 2.

Geo-mining conditions and hydrogeological conditions in the HCMA have been thoroughly explored by Huainan Mining Industry (Group) Co., Ltd. In addition, through outdoor sampling and indoor laboratory analysis, the detailed structural hierarchy of the alluvial soil layer and physical and mechanical parameters of the alluvial soil mass after mining subsidence disturbance were obtained. According to the field data from the HCMA, the depth of the groundwater level in the HCMA was  $h = 3$  m,  $\eta = 3 - 400$  m, the void ratio of the alluvial soil mass after mining subsidence disturbance was  $e_2 = 0.85$ , and the void ratio of the alluvial soil mass before mining disturbance was  $e_1 = 1.08$ . According to Eq. (20),  $\Delta e$  was calculated to be  $-0.23$ .

According to the data listed in Table 2, the subsidence coefficient obtained from the PIM (1.14) is greater than that obtained from the CPM (0.90); the difference between the two coefficients is 0.24. As mentioned previously, the measured ground surface subsidence in CMATASs contains four parts. However, because the PIM itself cannot reflect the role of the soil mass in mining subsidence, it is unable to separate the additional subsidence due to the alluvial soil mass from the measured data. Because the CPM already considers the compacting and consolidation subsidence of the alluvial soil, its subsidence coefficient is attributable solely to coal mining. Thus, it is reasonable for the CPM to have obtained a smaller coefficient value than the PIM.

The parameters and prediction models selected for the calculation are listed in Table 3, the calculation results are listed in Table 4, and the comparison of the prediction results with the measured data is shown in Fig. 17.

As can be seen from the results listed in Table 4, there are two small subsidence troughs caused by the compaction of alluvial soil in the edge region. The maximum

The whole overlying strata	Thickness	Columnar	Lithological description
	Min~Max Average		
Alluvial soil layer	420~440 430		Top: dark sandy clay, clay Central: clayey sand and sand powder Lower part: fine sand and sandy clay
			Consolidation of dense clay and fine sand, with more calcareous solid mass
			Mainly consolidated clay, including a thin layer of sand and clay sand
			Mainly consolidated clay, including a thin layer containing sand or clay
			Top: muddy gravel; Central: sandy clay and clay locally containing gravel; Lower: gravel and sandy clay layer including coarse clay.
Bedrock mass	31.6~51.7 41.7		Piebald mudstone, sandy mudstone in gray color, including thin-bedded fine-grained sandstone; the top contains the coal-bearing line or carbon shale
			15th coal seam
			Lime mudstone
			14th coal seam
			Gray sandy mudstone or light gray fine sandstone
			14th-1 coal seam
			Upper part consists of gray sandy mudstone
			Lower part consists of fine-grained sandstone
Mining coal seam	4.0~6.0 5.0		13th coal seam
Floor of coal seam	21.1~30.5 25.8		Mudstone, sandy mudstone and siltstone and fine inter-bedded sandstone thin sandstone at the bottom

Fig. 15 Borehole log of Pansan Mine in Huainan Coal Mining Area (HCMA)

compacting subsidence of the shallow soil mass is 39 mm, which accounts for 2.6% of the maximum subsidence, and forms two small basins in the boundary zone of the entire basin. The consolidation subsidence of the deep soil mass is 204 mm, accounting for 13.8% of the maximum subsidence. Therefore, the additional subsidence of the alluvial

soil mass is 243 mm, accounting for 16.4% of the total ground subsidence; thus, the additional subsidence cannot be ignored in the mining subsidence of CMATASs. Moreover, larger additional subsidence of the alluvial soil mass due to their relatively low groundwater levels exists in the Pingdingshan Coal Mining Area and Yanzhou Coal

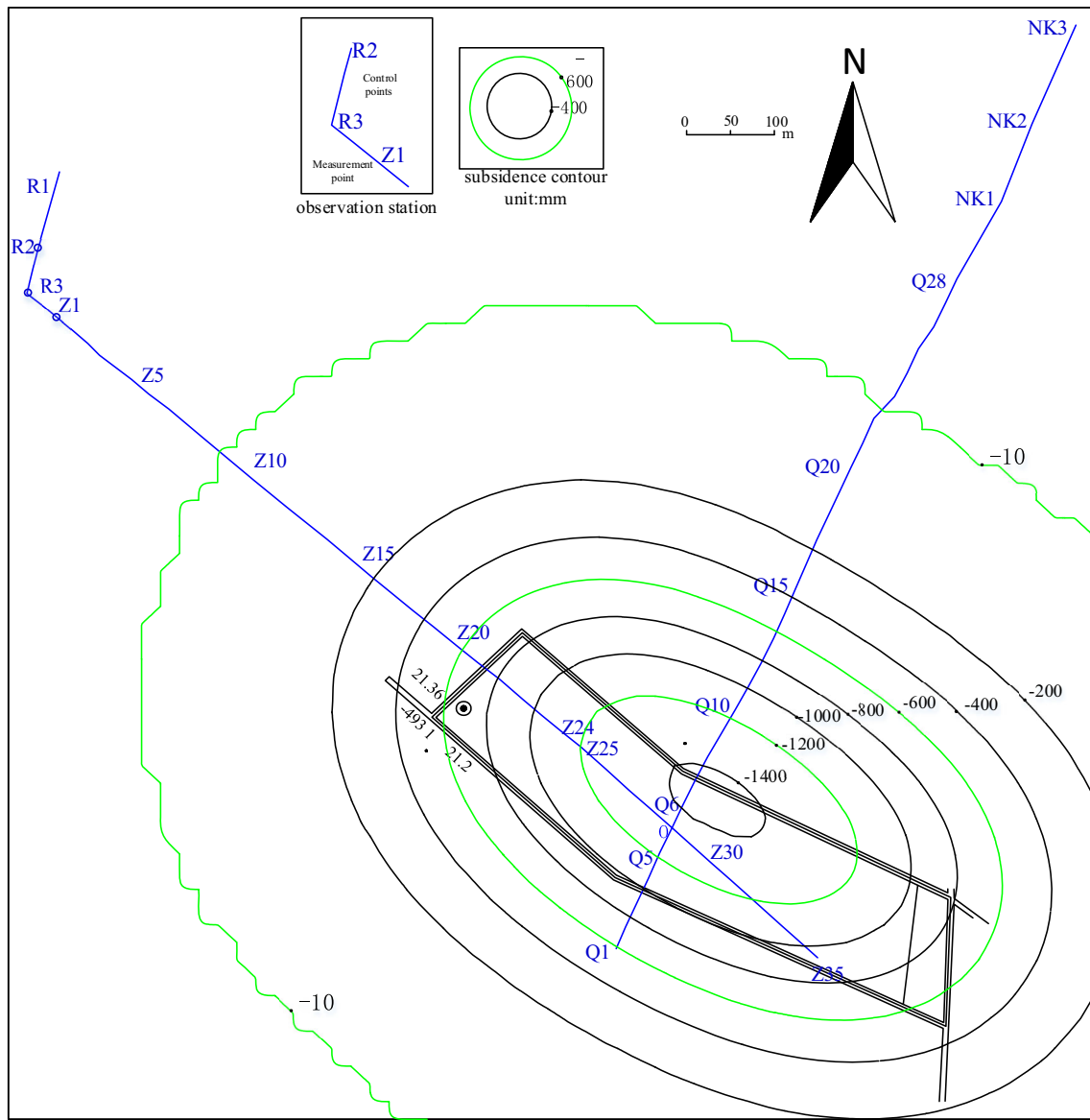


**Fig. 16** Layout of ground movement observation station on 1212(3) working face of Pansan Mine in North Area of HCMA

**Table 2** Measured subsidence factors for 1212(3) working face

	Subsidence coefficient	Tangent of major influence angle	Horizontal displacement coefficient	Propagation angle of extraction (°)	Deviation of inflection point			
					S <sub>1</sub>	S <sub>2</sub>	S <sub>3</sub>	S <sub>4</sub>
PIM	1.14	1.5	0.35	90	-6	4	-5	8
CPM	0.90	1.6	0.33	90	0	0	0	0

**Table 3** Selected calculation parameters and prediction models

Model	Parameters	Results	The contained contents of the results	Different areas of subsidence trough	Relative RMSE/K (%)
CPM	Parameters of CPM	“Subsidence calculated by CPM” in Table 4	Contains all the aforementioned four parts of subsidence	Entire region Middle region Edge region	4.9 5.0 4.7
PIM	Parameters of PIM	“Subsidence calculated by PIM” in Table 4	Not contain the compacting subsidence of alluvial soil	Entire region Middle region Edge region	6.0 6.5 5.3
PIM	Parameters of CPM	“Subsidence $W_{fs}$ ” in Table 4	Just contain the following subsidence and the synergy subsidence		

Mining Area of China. In addition, in the middle region of the subsidence trough, the fitting effect of the CPM (relative error of 5.0%) is better than that of the PIM (relative error of 6.5%). In the edge region of the subsidence trough, the fitting effect of the CPM (relative error of 4.7%) is also better than that of the PIM (relative error of 5.3%). Hence, the accuracy is improved by 11.3%. Considering the overall fitting effect in the entire region, the CPM demonstrates a better fitting effect in terms of the measured subsidence value, with a relative error of 4.9%, which is an 18% improvement over the relative error obtained when using the PIM (6.0%).

## Conclusions

In this study, we first analyzed the composition structure of the overlying stratum above coal mining working faces. The entire overburden stratum above the coal mining area is considered to be composed of an alluvial soil layer and a bedrock layer. In underground mining, alluvial soil has a major effect on ground subsidence. This effect is especially large and not negligible when the alluvial soil accounts for a large proportion in the entire overlying stratum of CMATASs.

In this study, the applicability of the most popular PIM used for CMATASs was analyzed. The basic premise and hypothesis of the PIM is based on the sandbox model. Alluvial soil differs from sand and rock mass; the compressible nature of alluvial soil is in opposition to the basic premise and hypothesis of the PIM. In addition, according to field-measured ground subsidence data collected from 11 working faces in the North Area, the PIM was found not to be suitable for ground subsidence prediction in CMATASs, for two main reasons: (1) the subsidence basin range predicted by the PIM was smaller than the measured range;

thus, the predicted basin converged more rapidly than the measured basin at the edges. (2) Poor fitting results were obtained at the subsidence basin edge.

We thoroughly analyzed the mining-induced deformation inside the rock mass and alluvial soil and the crack (void) distribution within the rock mass due to underground coal mining. We obtained the mechanism of mining subsidence in CMATASs and the reasons why the PIM is not suitable for CMATASs. The research results indicate that the alluvial soil is compacted and then subsides under vertical compression deformation, which increases the ground subsidence. The bedrock is subjected to the weight/load of the thick alluvial soil layer. Because of the vertical compression deformation inside the rock, its internal voids (spaces) are compacted; thus, the replaced voids (spaces) are transferred to the ground surface, resulting in an increase in the ground subsidence. However, the effect of the alluvial soil on the ground subsidence cannot be detected by the PIM; moreover, the PIM is unable to represent the mechanism of the mining subsidence in CMATASs. Thus, the PIM cannot be used for predicting subsidence in CMATASs.

Based on the above research results, to precisely calculate the subsidence in CMATASs, we proposed a CPM for the mining subsidence in CMATASs based on soil mechanics and stochastic medium theory. The new CPM was applied to the mining process in the HCMA. The calculation results show that the maximum compacting subsidence of the shallow soil mass is 39 mm, which accounts for 2.6% of the maximum subsidence, and forms two small basins in the boundary zone of the entire basin. The consolidation subsidence of the deep soil mass is 204 mm, accounting for 13.8% of the maximum subsidence, and the additional subsidence of the alluvial soil mass is 243 mm, accounting for 16.4% of the total ground subsidence. The subsidence predicted by the CPM better



**Table 4** Measured subsidence and predicted subsidence

Points No.	Measured subsidence /mm	Subsidence calculated by PIM /mm	Subsidence $W_{fs}$ /mm	Subsidence $W_c$ /mm	Subsidence $W_l$ /mm	Subsidence calculated by CPM /mm
Z6	51	0	0	0	0	0
Z7	62	1	0	1	0	1
Z8	67	2	1	2	0	3
Z9	76	4	1	4	0	5
Z10	-	8	3	8	0	11
Z11	91	14	5	10	1	16
Z12	98	24	10	12	2	24
Z13	103	41	19	18	3	40
Z14	118	65	35	25	6	66
Z15	156	101	59	32	10	101
Z16	205	154	101	36	16	153
Z17	260	212	150	33	24	207
Z18	-	291	221	25	35	281
Z19	460	380	302	22	48	372
Z20	-	495	412	17	66	495
Z21	680	616	531	11	85	627
Z22	786	739	655	4	105	764
Z23	926	885	803	3	129	935
Z24	-	987	904	1	145	1050
Z24'	-	1098	1014	0	163	1177
Z25	1311	1178	1091	0	175	1266
Z26	-	1277	1179	0	189	1368
Z27	1415	1342	1237	0	198	1435
Z28	1449	1379	1267	0	203	1470

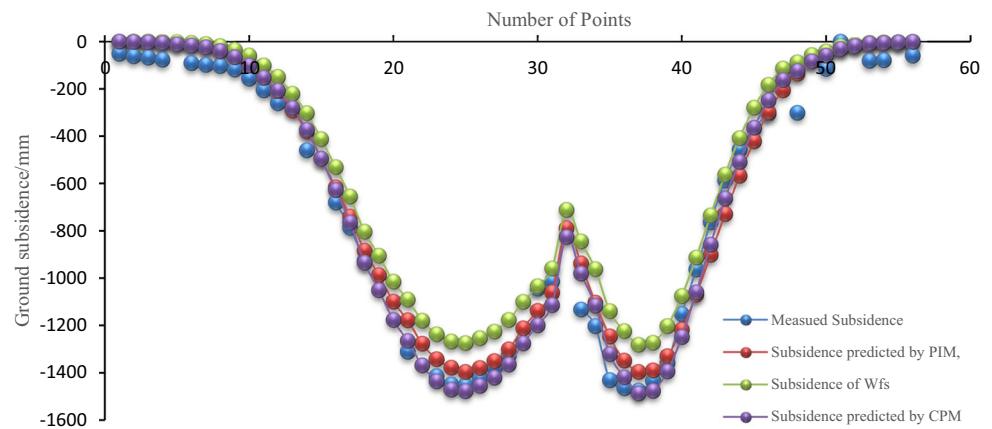
Small basins

Table 4 continued

Points No.	Measured subsidence /mm	Subsidence calculated by PIM /mm	Subsidence Wfs /mm	Subsidence Wc /mm	Subsidence Wl /mm	Subsidence calculated by CPM /mm
Z29	1454	1396	1274	0	204	1478
Z30	1424	1379	1254	0	201	1455
Z31	1378	1350	1225	0	196	1421
Z32	1324	1300	1176	0	188	1364
Z33	-	1211	1100	0	176	1276
Z34	1044	1137	1033	0	165	1198
Z35	1013	1061	960	0	154	1114
Q1	-	788	712	0	114	826
Q2	1132	938	845	0	135	980
Q3	1202	1103	961	0	154	1115
Q4	1431	1246	1138	0	182	1320
Q5	1465	1347	1223	0	196	1419
O	1475	1396	1281	0	205	1486
Q6	1435	1390	1273	0	204	1477
Q7	1359	1329	1202	0	192	1394
Q8	1151	1217	1076	0	172	1248
Q9	963	1069	913	1	146	1060
Q10	763	901	735	5	118	858
Q11	586	729	562	11	90	663
Q12	457	567	408	35	65	508
Q13	366	420	280	39	45	364
Q14	305	298	183	37	29	249
Q15	-	205	114	31	18	163
Q16	301	136	87	23	14	124
Q17	-	85	57	16	10	83
Q18	115	52	42	10	7	59
Q19	-	30	21	6	3	30
Q20	51	17	13	4	2	19
Q21	81	9	5	2	1	8
Q22	79	5	4	1	1	6
Q23	-	3	2	1	0	3
Q24	59	1	1	0	0	1

Small basins

**Fig. 17** Comparison of prediction results with measured data



fits the measured subsidence values, with a relative error of 4.9%, and the fitting accuracy is improved by 18% compared to the relative error of the PIM (6.0%). Thus, the proposed CPM is more suitable for predicting the ground subsidence caused by underground coal mining in CMATASs, and can be used to provide more accurate predictions for ground subsidence in similar coal mining areas.

**Acknowledgements** This research has been financially supported by the National Natural Science Foundation of China (Grant Numbers: 51604266, 51504239 and U1361203), the Natural Science Foundation of Jiangsu province (BK20150187), the Priority Academic Program Development of the Jiangsu Higher Education Institutions (PAPD). The authors express their special thanks to the research and support provided by Huainan Mining Industry (Group) Co., Ltd., and the National Engineering Lab of Coal Ecological Environment Protection. The financial support from all the above mentioned sources is gratefully acknowledged. The authors are also grateful to the reviewers of this paper for their comments.

## References

- Alejano LR, Ramirez-Oyanguren P, Taboada J (1999) FDM predictive methodology for subsidence due to flat and inclined coal seam mining. *Int J Rock Mech Min Sci* 36:475–491. doi:10.1016/S0148-9062(99)00022-4
- Asadi A, Shakhriar K, Goshtasbi K (2004) Profiling function for surface subsidence prediction in mining inclined coal seams. *J Min Sci* 40:142–146
- Asadi A, Shahriar K, Goshtasbi K, Najm K (2005) Development of a new mathematical model for prediction of surface subsidence due to inclined coal-seam mining. *J South Afr Ins Min Metall* 105:15–20
- Baochen L, Ronggui Y (1981) The basic rules of displacement of rock mass due to underground mining. *J China Coal Soc* 1:40–55
- Brady BHG, Brown ET (2004) *ROCK mechanics for underground mining*, 3rd edn. Springer, Dordrecht
- Bureau HCM, Mine LTZC, Branch TC (1983) Mining under the Huaihe River and its embankment (in Chinese). *Mine Surv* 1:26–33
- Cui XM, Fang ZH, Zuo HF, Li HX (2000a) effect of aquifer water loss caused by underground mining on the surface subsidence. *Coal Geol Explor* 28:47–48
- Cui XM et al (2000b) Improved prediction of differential subsidence caused by underground mining. *Int J Rock Mech Min Sci* 37:615–627. doi:10.1016/S1365-1609(99)00125-2
- Cui XM, Wang JC, Liu Y (2001) Prediction of progressive surface subsidence above longwall coal mining using a time function. *Int J Rock Mech Min Sci* 38:1057–1063
- Djamaluddin I, Mitani Y, Esaki T (2011) Evaluation of ground movement and damage to structures from Chinese coal mining using a new GIS coupling model. *Int J Rock Mech Min Sci* 48:380–393. doi:10.1016/j.ijrmms.2011.01.004
- Ge X, Yu G (2006) Influence of underground mining on ground surface and railway bridge under thick alluvium. *J China Univ Min Technol* 16:97–100
- Gong X (1996) *Advanced soil mechanics*. Zhejiang University Press, Hang Zhou
- Hao Q (1988) Void diffusion model for mined strata and analysis of influence of void sources (in Chinese). *J China Univ Min Technol* 02:30–36
- Hao Q, Ma W (1985) On the methods of ground subsidence prediction (in Chinese). *J China Univ Min Technol* 02:37–42
- Hao Q, Ma W (1986) The optimum form of weibull distribution subsidence equation and its application in surface subsidence calculation (in Chinese). *J China Univ Min Technol* 03:32–42
- He G (1982) Application of influence function of Weber distribution to the precalculation of ground surface movement: a study on the fundamental law of ground movement based on the elastic theory. *J China Univ Min Technol* 1:1–20
- He G, Yang L, Ling G, Jia C, Hong D (1991) *Mining subsidence science*. China University of Mining and Technology Press, Xuzhou
- Huayang D, Xugang L, Jiyan L, Yixin L, Yameng Z, Weinan D, Yinfei C (2010) Model study of deformation induced by fully mechanized caving below a thick loess layer. *Int J Rock Mech Min Sci* 47:1027–1033
- Holla L (1997) Ground movement due to longwall mining in high relief areas in New South Wales, Australia. *Int J Rock Mech Min Sci* 34:775–787
- Kratzsch H (1983) *Mining subsidence engineering*. Springer, Berlin
- Li L, Wu K, Zhou DW (2014) AutoCAD-based prediction of 3D dynamic ground movement for underground coal mining. *Int J Rock Mech Min Sci* 71:194–203. doi:10.1016/j.ijrmms.2014.04.025
- Liang Q, Wen X, He G, Chen Q, Yang J (2007) Study on calculation methods for surface subsidence caused by water loss of clay. *J Min Safety Eng* 24:105–108
- Litwiniszyn J (1956) Application of the equation of stochastic processes to mechanics of loose bodies. *Arch Mech Stos* 8:393–411

- Litwiniszyn J (1974) Stochastic methods in mechanics of granular bodies. Springer, Vienna
- Liu Y (1981) Surface movements, overburden failure and its application. Coal Industry, Beijing
- Liu Y, Dai H, Jiang Y (2012) Model test for mining-induced movement law of rock and soil mass under thick unconsolidated layers. *J Min Safety Eng* 29:268–272
- Miao X, Cui X, Ja W, Xu X (2011) The height of fractured water-conducting zone in undermined rock strata. *Eng Geol* 120:32–39. doi:[10.1016/j.enggeo.2011.03.009](https://doi.org/10.1016/j.enggeo.2011.03.009)
- Peng SS (1992) Surface subsidence engineering. Littleton Society for Mining, Metallurgy, New York
- Peng S, Zhang J (2007) Engineering geology for underground rocks. Springer, Berlin
- Qian MG (1982) A study of the behavior of overlying strata in longwall mining and its application to strata control. Paper presented at the Proceedings of the Symposium on Strata Mechanics, New York
- Qian M, Miao X, Xu J, Mao X (2003) Study of key strata theory in ground control. China University of Mining and Technology Press, Xuzhou
- Qian MG, Shi PW, Xu JL (2010) mining pressure and strata control. China University of Mining and Technology Press, Xuzhou
- Reddish DJ, Whittaker BN (2012) Subsidence occurrence, prediction and control, vol 56. Elsevier, Amsterdam
- Sheorey PR, Loui JP, Singh KB, Singh SK (2000) Ground subsidence observations and a modified influence function method for complete subsidence prediction. *Int J Rock Mech Min Sci* 37:801–818. doi:[10.1016/S1365-1609\(00\)00023-X](https://doi.org/10.1016/S1365-1609(00)00023-X)
- Singh RP, Yadav RN (1995) Prediction of subsidence due to coal mining in Raniganj coalfield, West Bengal, India. *Eng Geol* 39:103–111
- State Bureau of Coal Industry (2004) The regulation of leaving coal pillar and mining coal of holding under the buildings, water bodies, railways and the main roadway. Coal Industry, Beijing
- Sui W (1992) Mechanism and prediction of soil mass deformation due to mining subsidence (in Chinese). China University of Mining and Technology, Xuzhou
- Tan Z, Deng K, Yang J (2002) Research on ground movement laws for strip mining under thick alluvium. *J China Univ Min Technol* 12:61–64
- Wu K, Ge J, Wang LD, Zhou M (1998) Unify method of mining subsidence prediction. China University of Mining and Technology Press, Xuzhou
- Wu K, Deng K, Zhou M, Huang Z, Zheng Y, Wang Z (1999) The analysis of monitor conclusion about overburden displacement under condition of fully mechanized sublevel caving. *J China Coal Soc* 24:21–24
- Wu K, Jin J, Dai Z, Jiang J (2002) The experimental study on the transmit of the mining subsidence in soil. *J China Coal Soc* 27:601–603
- Wu Q, Fan S, Zhou W, Liu S (2013) Application of the analytic hierarchy process to assessment of water Inrush: a case study for the No. 17 Coal Seam in the Sanhejian Coal Mine. *China Mine Water Environ* 32:229–238
- Xu Z (2006) Elastic mechanics. Higher Education, Beijing
- Yin Z (2007) The principle of geotechnical engineering. China Water Power, Beijing
- Yuan L, Wu K (2003) Theoretical research and technology practice on mining under the Huaihe River embankment. China University of Mining and Technology Press, Xuzhou
- Zhang X, Zhao Y, Liu S (1999) A new method of calculating surface subsidence and deformations under thick alluvial soil the Chinese. *J Nonfer Metals* 9:435–440
- Zhou DW (2014) The synergy mechanism between rock mass and soil in mining subsidence and its prediciton (in Chinese). China University of Mining and Technology Press, Xuzhou
- Zhou DW, Wu K, Cheng GL, Li L (2015) Mechanism of mining subsidence in coal mining area with thick alluvium soil in China. *Arab J Geosci* 8:1855–1867. doi:[10.1007/s12517-014-1382-2](https://doi.org/10.1007/s12517-014-1382-2)
- Zhou D, Wu K, Li L, Diao X, Kong X (2016a) A new methodology for studying the spreading process of mining subsidence in rock mass and alluvial soil: an example from the Huainan coal mine, China. *Bull Eng Geol Environ* 75:1067–1087. doi:[10.1007/s10064-016-0877-3](https://doi.org/10.1007/s10064-016-0877-3)
- Zhou DW, Wu K, Li L, Yu JW (2016b) Impact of thick alluvial soil on a fractured water-conducting zone: an example from Huainan coal mine, China. *J South Afr Inst Min Metall* 116:431–440. doi:[10.17159/2411-9717/2016/v116n5a9](https://doi.org/10.17159/2411-9717/2016/v116n5a9)